Electronic Supplementary Information

A Simple Quinolone Schiff-Base Containing CHEF Based Fluorescence 'turn-on' Chemosensor for Distinguishing Zn^{2+} and Hg^{2+} with High Sensitivity, Selectivity and Reversible

Yuwei Dong,[a] Ruiqing Fan,*[a] Wei Chen,[a] Ping Wang,[a] and Yulin Yang,*[a]

MIIT Key Laboratory of Critical Materials Technology for New Energy Conversion and Storage, School of Chemistry and Chemical Engineering, Harbin Institute of Technology, Harbin 150001 (P. R. China)

E-mail: fanruiqing@hit.edu.cn and ylyang@hit.edu.cn

Index

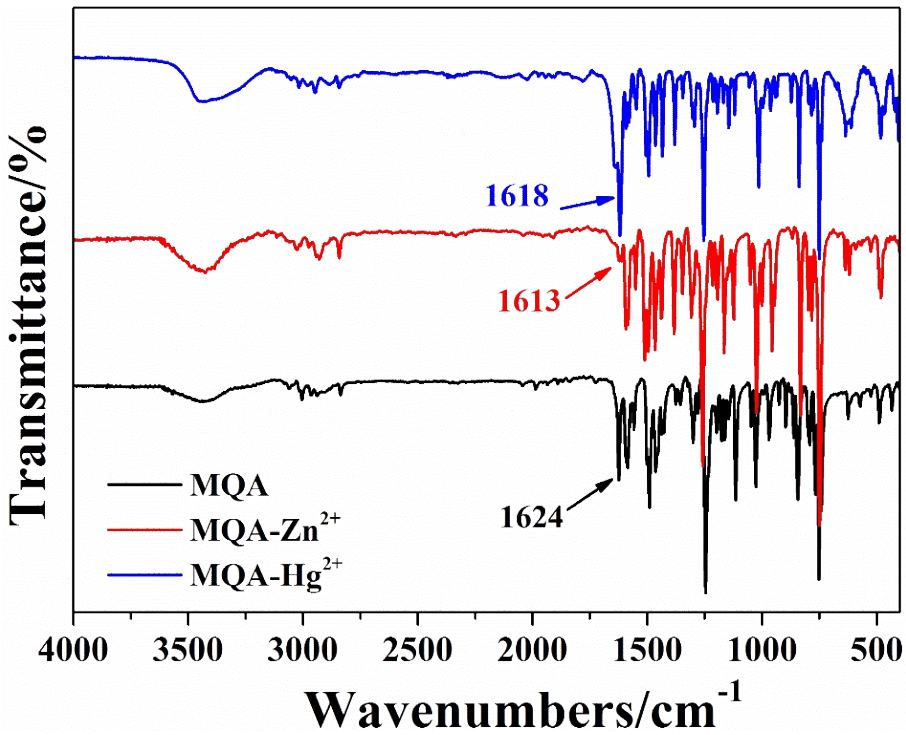

Figure S1. IR spectra of chemosensor **MQA** and complexes **MQA-Zn^{2+}**, **MQA-Hg^{2+}** in KBr disks.

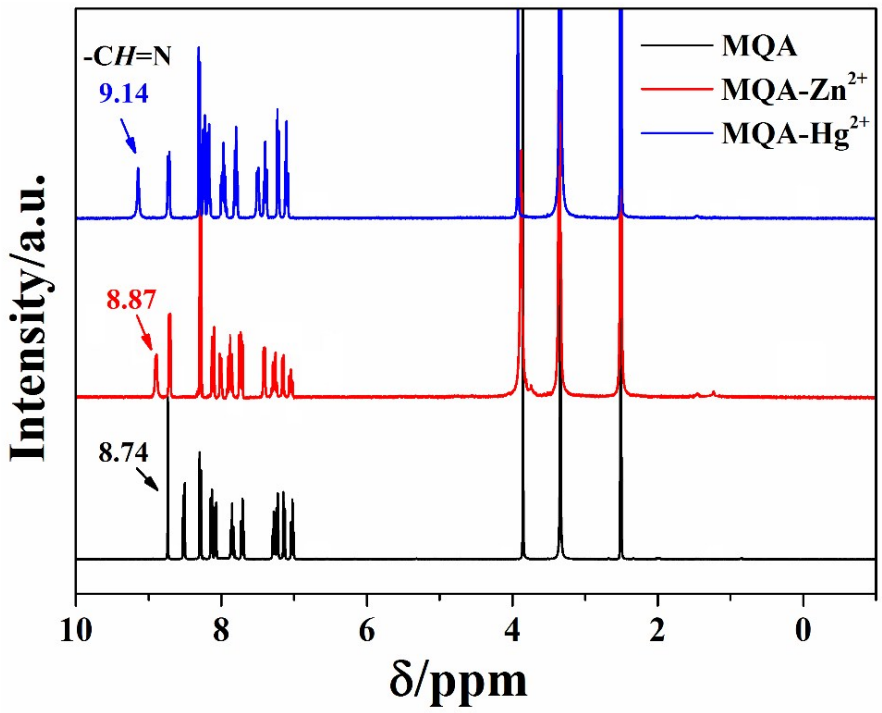

Figure S2. ^{1}H NMR spectra of chemosensor **MQA** and complexes **MQA-Zn^{2+}**, **MQA-Hg^{2+}** in d_6-DMSO.

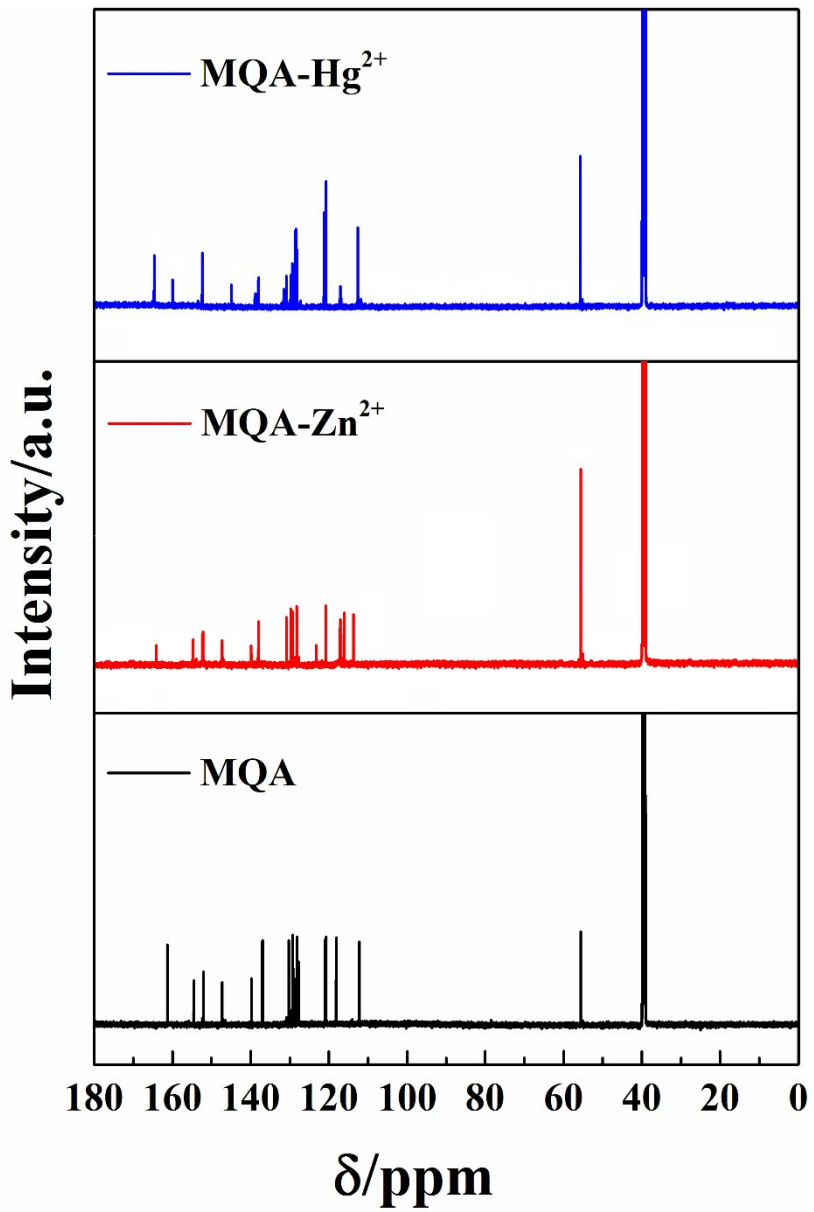

Figure S3. ^{13}C NMR spectra of chemosensor **MQA** and complexes **MQA-Zn^{2+}**, **MQA-Hg^{2+}** in d_6-DMSO.

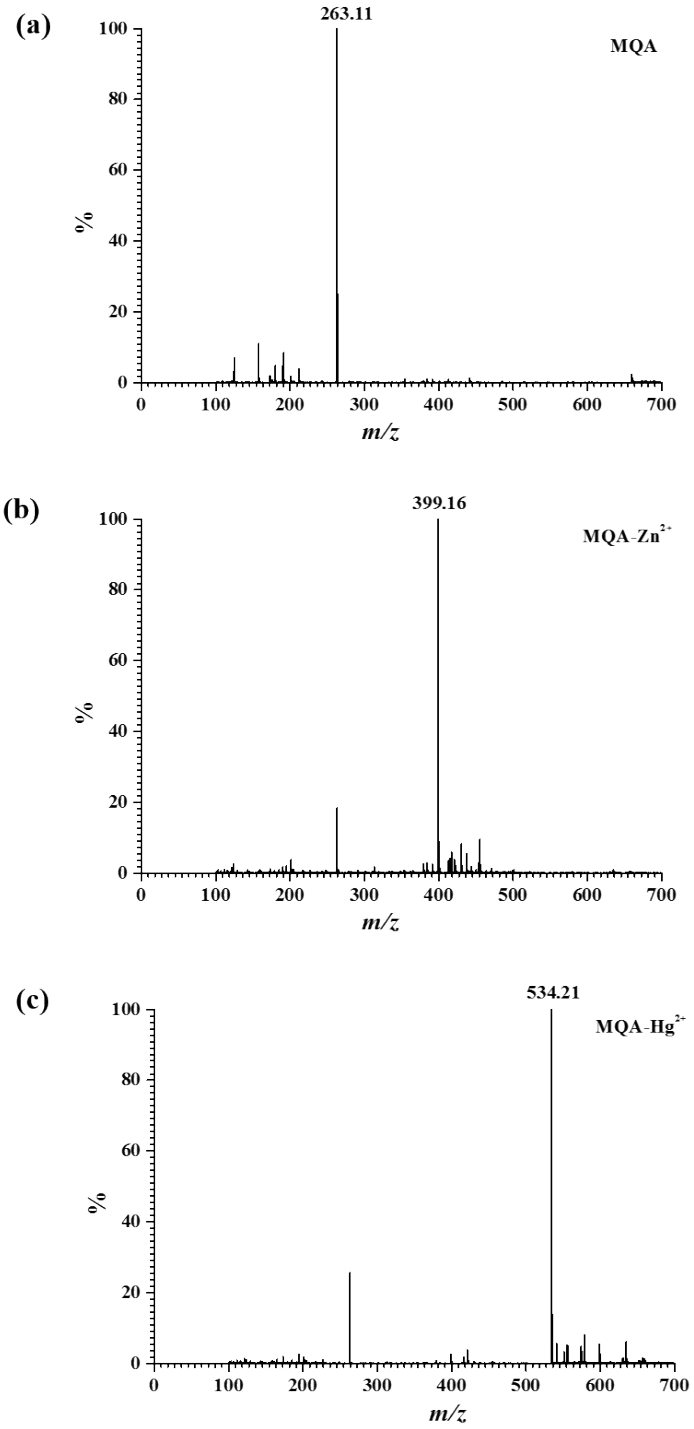

Figure S4. ESI-MS spectra of (a) **MQA**, (b) **MQA-Zn^{2+}** and (c) **MQA-Hg^{2+}**.

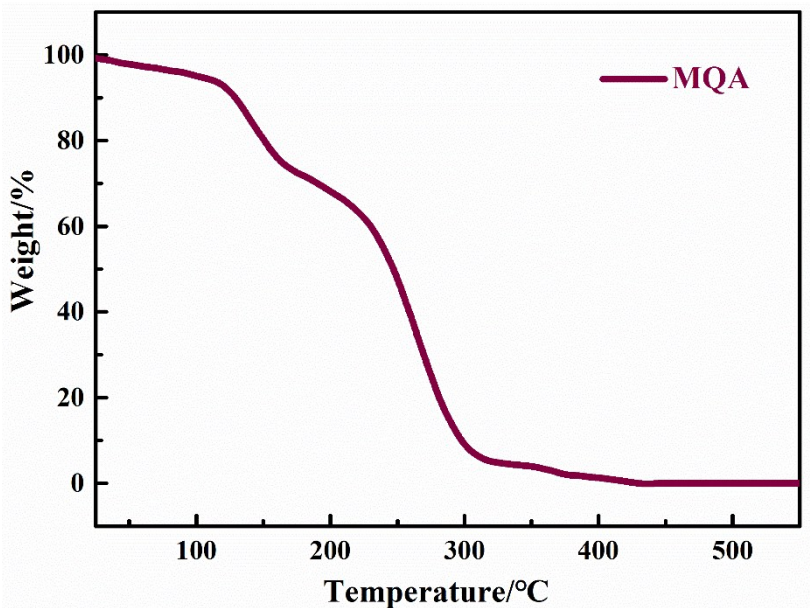

Figure S5. Thermal gravimetric curve of chemosensor **MQA**.

Association constant (K_a) calculation

Assuming a 1:1 complex formation, the association constant was calculated on the basis of the titration curves of the chemosensor **MQA** with M^{2+} (Zn^{2+}/Hg^{2+}). The association constant was calculated according to the Benesi–Hildebrand equation (1):

$$\frac{1}{I - I_0} = \frac{1}{K_a(I_{max} - I_0)[M]^n} + \frac{1}{I_{max} - I_0} \tag{1}$$

Where K_a is complex association constant, I_0 is the fluorescent intensity of **MQA** in the absence of M^{2+}, I is the fluorescent intensity recorded in the presence of added M^{2+}, I_{max} is the fluorescent intensity in presence of added $[M^{2+}]_{max}$, and n is the binding stoichiometry ratio between **MQA** and M^{2+} (Zn^{2+}/Hg^{2+}). The association constant (K_a) could be determined from the slope of the straight line of the plot of $1/(I - I_0)$ against $1/[M]^n$.

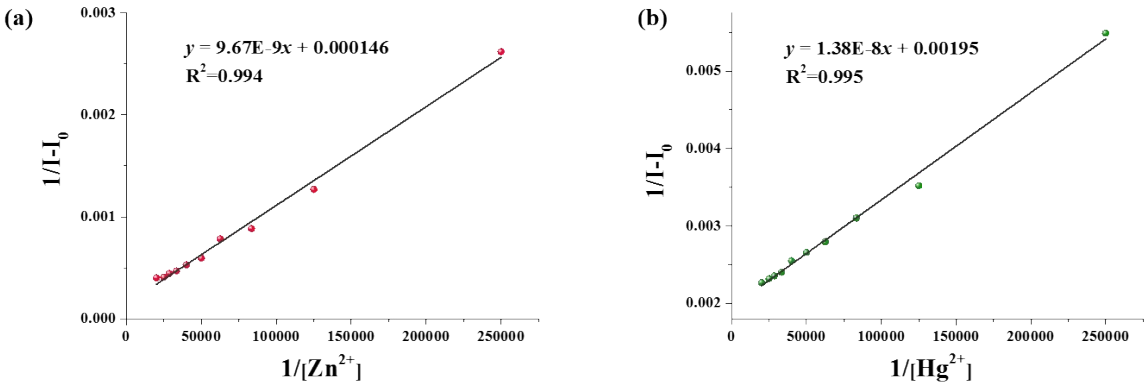

Figure S6. (a) Benesi-Hildebrand equation plot (fluorescence intensity at 565 nm) of **MQA**, assuming 1:1 stoichiometry for association between **MQA** and Zn^{2+}. (b) Benesi-Hildebrand equation plot (fluorescence intensity at 530 nm) of **MQA**, assuming 1:1 stoichiometry for

association between **MQA** and Hg^{2+}.

Standard deviation and detection limit calculation

The detection limit was calculated based on the fluorescence titration. To determine the S/N ratio, fluorescence intensity of **MQA** without M^{2+} (Zn^{2+}/Hg^{2+}) was measured by five times and the standard deviation of blank measurements was determined. To gain the slop, the fluorescence intensity data at 565 nm and 530 nm for Zn^{2+} and Hg^{2+}, respectively, were plotted as a concentration of M^{2+}. So the detection limit was calculated with the follow equation (2):

$$\text{Detection limit} = 3\sigma/m \quad (2)$$

Where σ is the standard deviation of blank measurements, and m is the slop of fluorescence versus M^{2+} concentration.

Table S1. Standard deviation calculation.

	Fluorescence intensity
Test 1	28.20
Test 2	28.68
Test 3	27.09
Test 4	30.40
Test 5	29.85
Standard Deviation (σ)	1.32

Table S2. Detection limit calculation.

	Detection Zn^{2+}	Detection Hg^{2+}
Slope (m)	117.79 μM^{-1}	32.65 μM^{-1}
Detection limit (3σ/m)	0.011 μM	0.040 μM

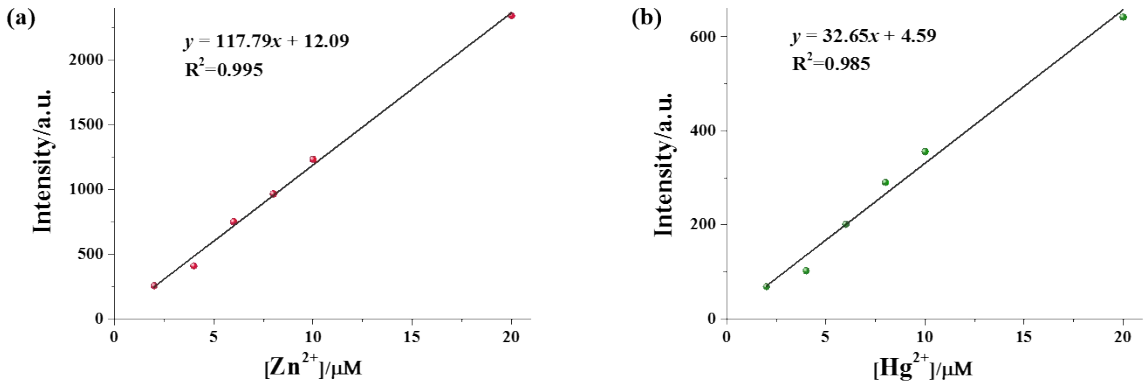

Figure S7. (a) Plot of fluorescence intensity of **MQA** with Zn^{2+} at 565 nm. (b) Plot of fluorescence intensity of **MQA** with Hg^{2+} at 530 nm.

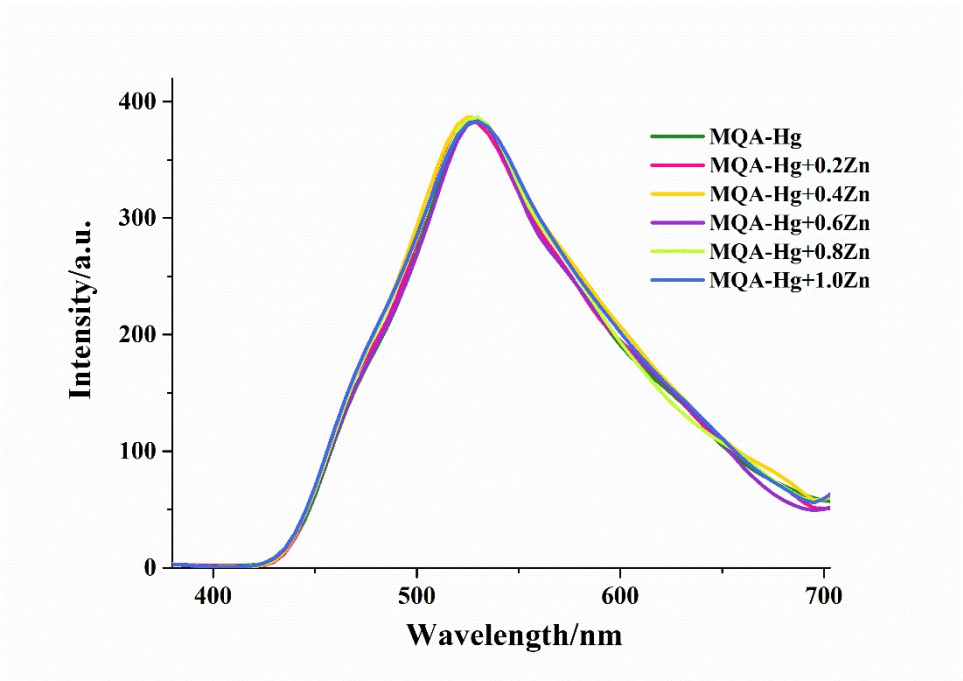

Figure S8. Fluorescence spectra of **MQA** (10 μM) with Hg^{2+} (1.0 equiv.) upon titration of Zn^{2+} (0.2, 0.4, 0.6, 0.8 and 1.0 equiv.).

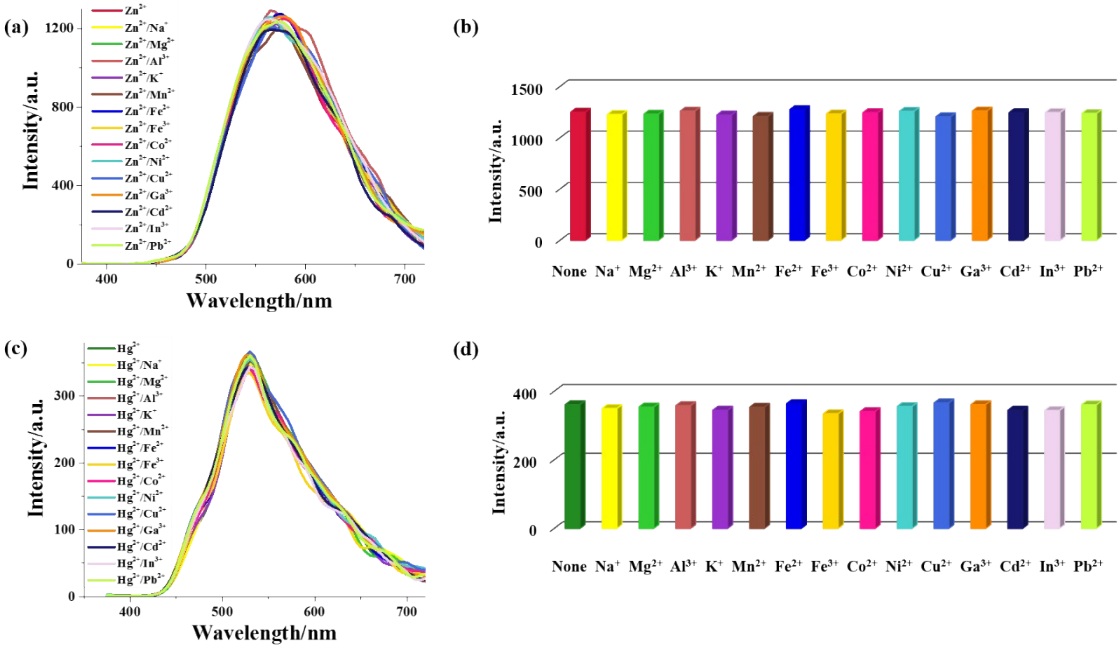

Figure S9. (a) Fluorescence spectra and (b) fluorescence intensity change of Zn^{2+}-bound **MQA** in DMSO/water mixture (1/99 v/v) in the presence other metal ions. (c) Fluorescence spectra and (d) fluorescence intensity change of Hg^{2+}-bound **MQA** in DMSO/water mixture (1/99 v/v) in the presence other metal ions.

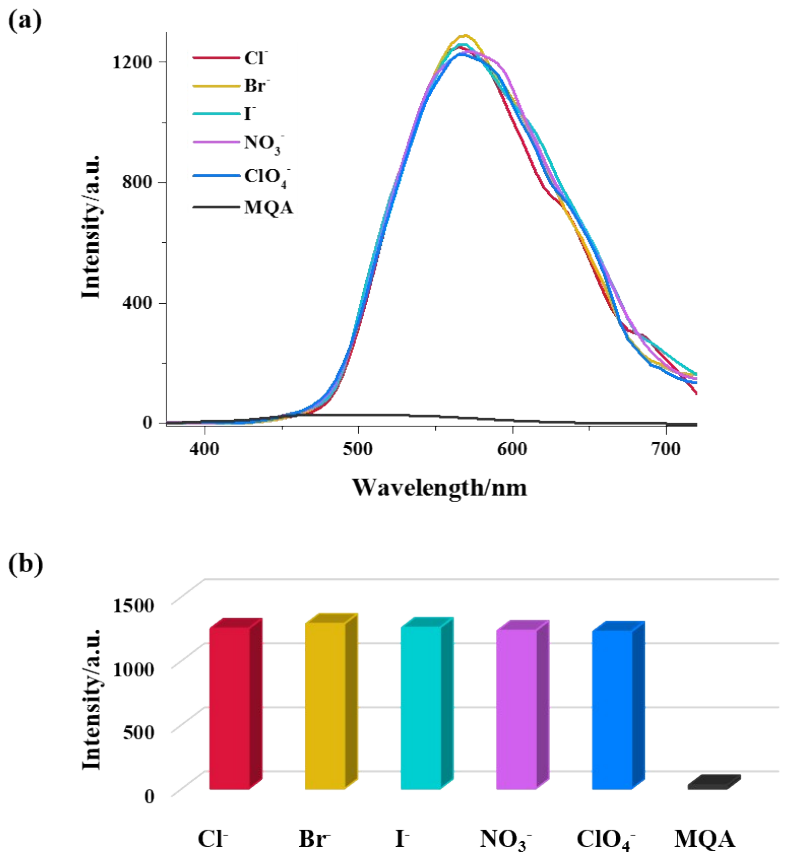

Figure S10. (a) Fluorescence spectra and (b) fluorescence intensity change of Zn^{2+}-bound **MQA** in DMSO/water mixture (1/99 v/v) with different anions.

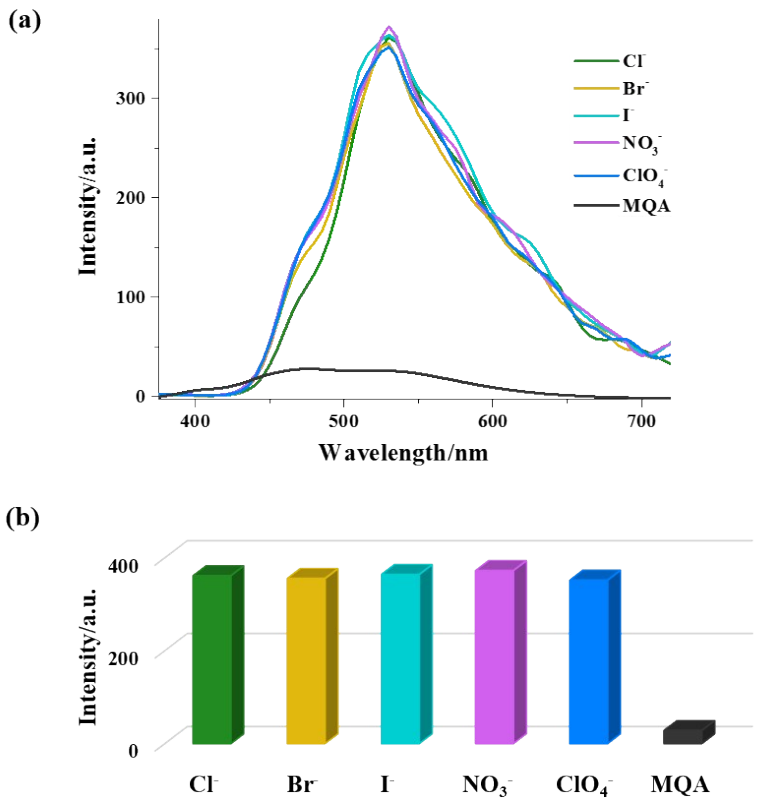

Figure S11. (a) Fluorescence spectra and (b) fluorescence intensity change of Hg^{2+}-bound **MQA** in DMSO/water mixture (1/99 v/v) with different anions.

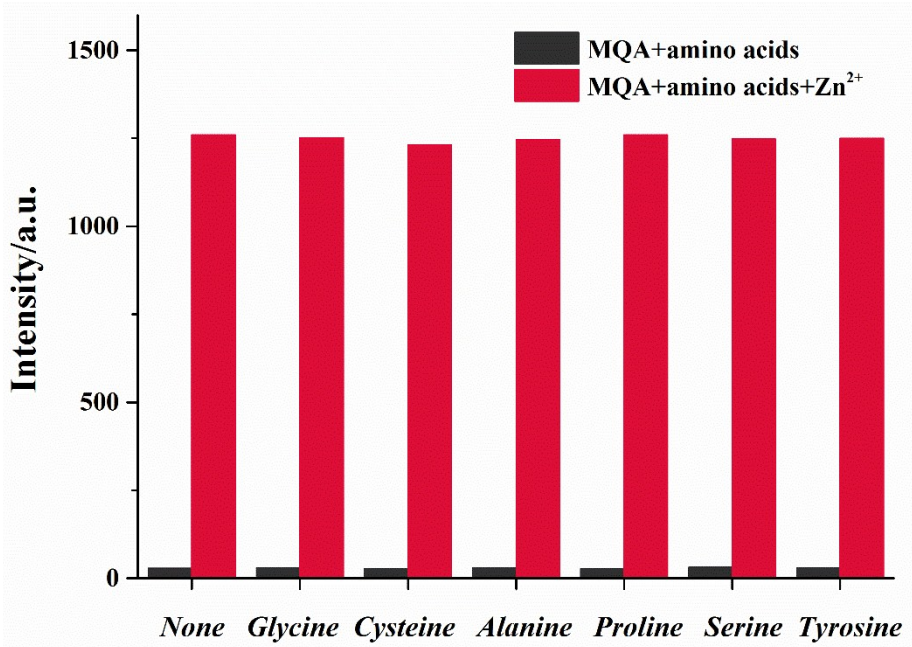

Figure S12. Fluorescence response ($I_{565\ nm}$) of Zn^{2+} sensing by **MQA** (10 μM) with various amino acids (2.0 equiv.) in DMSO/water mixture (1/99 v/v). The black bars represent the addition 2.0 equiv. of the various amino acids to a 10 μM solution of **MQA**. The red bars represent the change of the emission that occurs upon the subsequent addition of 1.0 equiv. Zn^{2+} to the above solution.

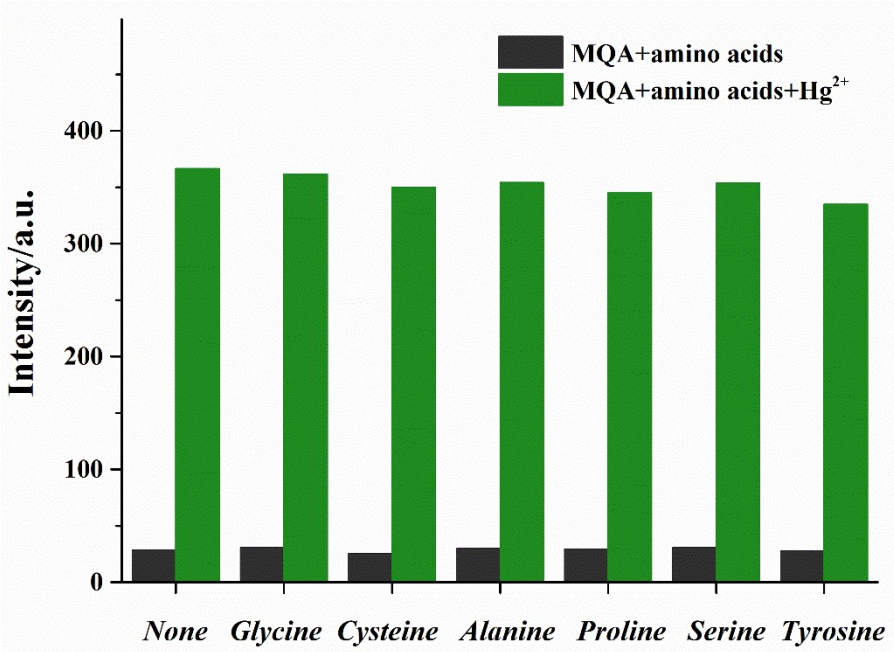

Figure S13. Fluorescence response ($I_{530\ nm}$) of Hg^{2+} sensing by **MQA** (10 μM) with various amino acids (2.0 equiv.) in DMSO/water mixture (1/99 v/v). The black bars represent the addition 2.0 equiv. of the various amino acids to a 10 μM solution of **MQA**. The red bars represent the change of the emission that occurs upon the subsequent addition of 1.0 equiv. Hg^{2+} to the above solution.

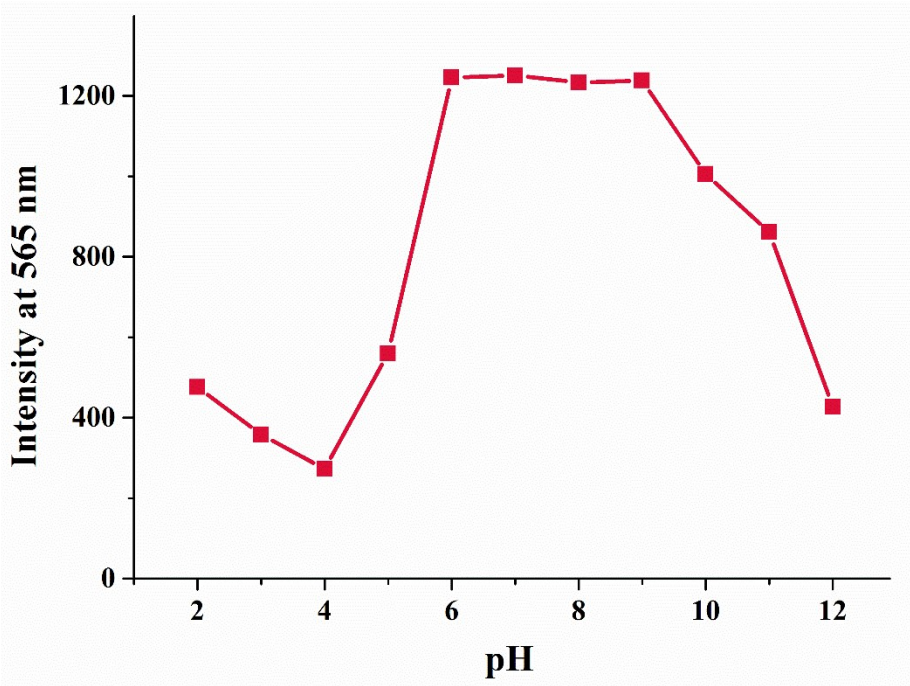

Figure S14. Changes in fluorescence intensity of **MQA** (10 μM) measured with Zn^{2+} (1.0 equiv.) as a function of pH at room temperature.

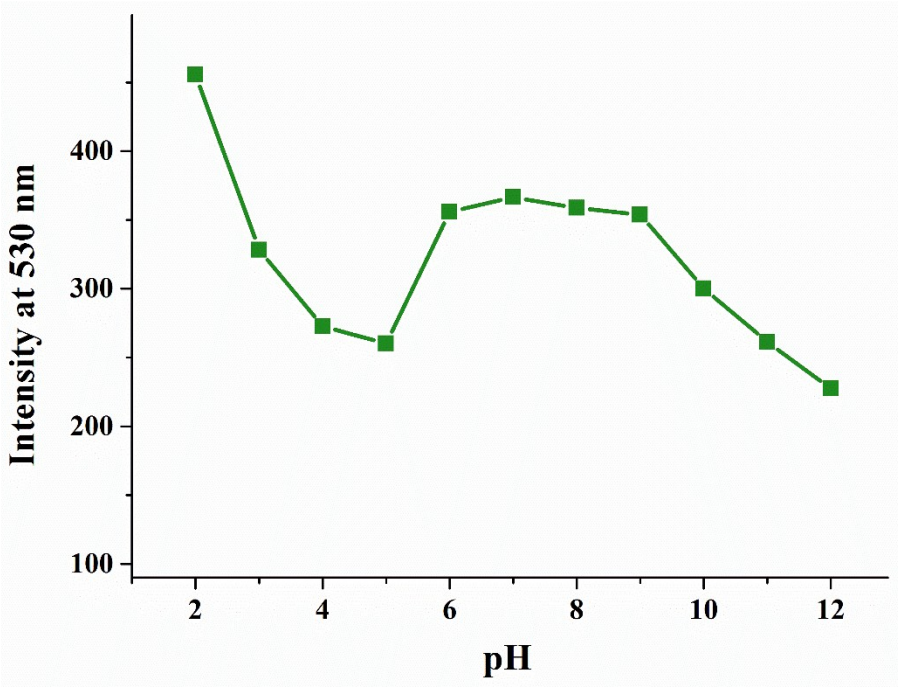

Figure S15. Changes in fluorescence intensity of **MQA** (10 μM) measured with Hg^{2+} (1.0 equiv.) as a function of pH at room temperature.

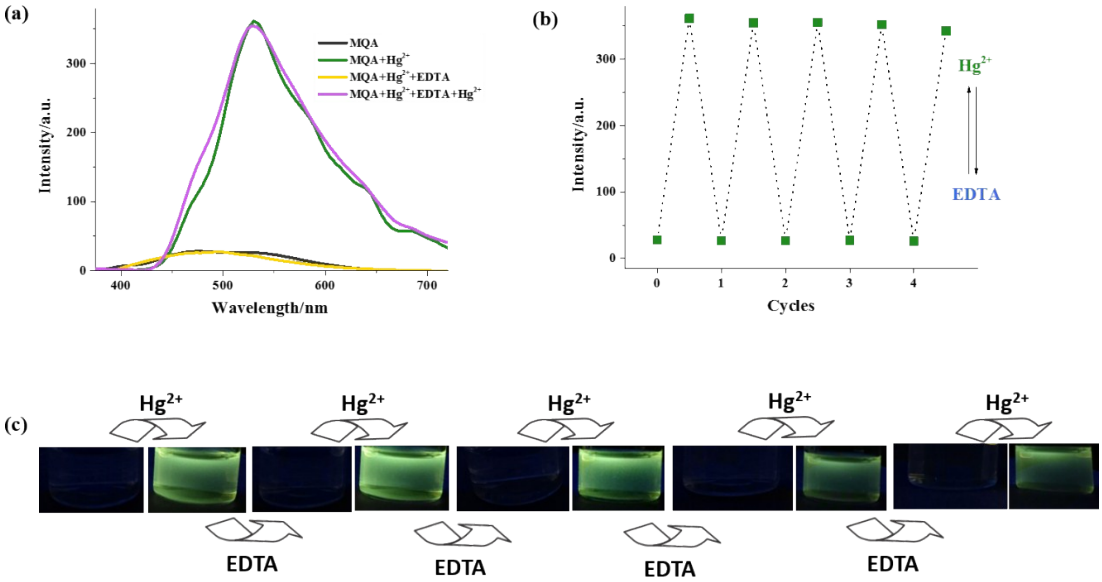

Figure S16. (a) Fluorescence spectral changes of **MQA** (10 μM) after the sequential addition of Hg^{2+} and EDTA in buffer solution (bis–tris, pH 7.0). (b) Reversible changes in fluorescence intensity and (c) luminescent photos of **MQA** (excitation under a 365 nm UV lamp) after the sequential addition of Hg^{2+} and EDTA.

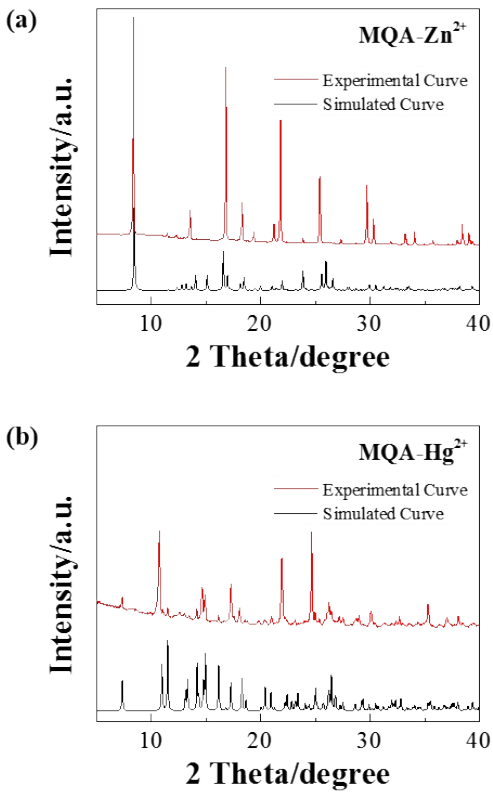

Figure S17. Experimental (top) and simulated (bottom) PXRD patterns of complexes **MQA-Zn^{2+}** (a) and **MQA-Hg^{2+}** (b).

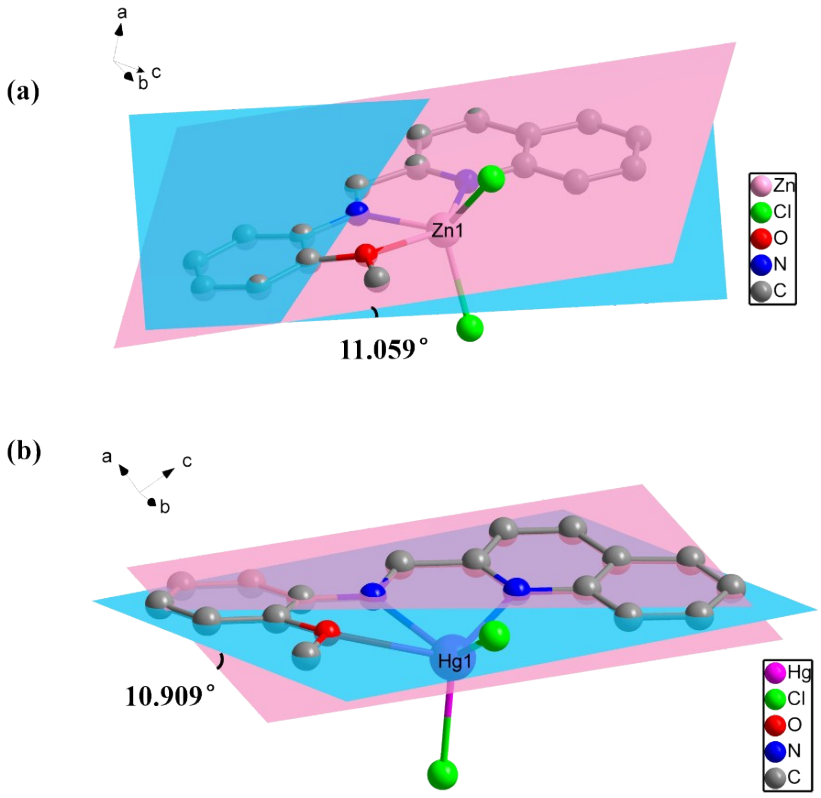

Figure S18. Depiction of the dihedral angle between the phenyl ring and quinolone ring in complexes **MQA-Zn^{2+}** (a) and **MQA-Hg^{2+}** (b).

Table S3. Comparison of a few aspects of some recently published Zn-sensors.

Chemosensor	No. of steps for synthesis	Detection Limit (μM)	Binding constant (M^{-1})	Percent of water in solution	Reference
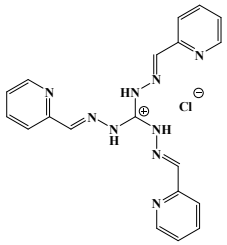	1	2.5	1.9×10^5 (Zn1) 1.5×10^4 (Zn2) 6.1×10^3 (Zn3)	100%	[S1]
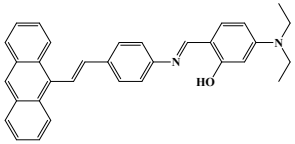	5	0.0719	1.05×10^6	0 (100% methanol)	[S2]
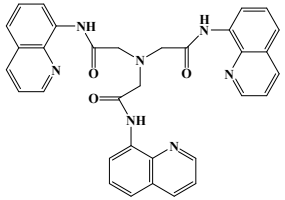	4	3.2	4×10^4	0 (5% acetonitrile)	[S3]
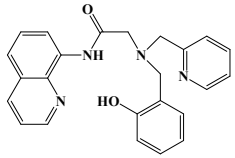	3	0.066	1.4×10^6	0 (100% acetonitrile)	[S4]
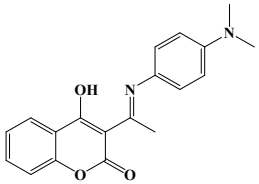	1	65.41	4.8×10^5	50%	[S5]

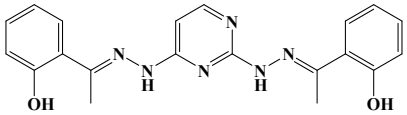	1	0.69	11.82×10^4	20%	[S6]
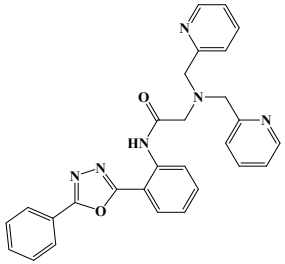	2	0.86	2.82×10^8	100%	[S7]
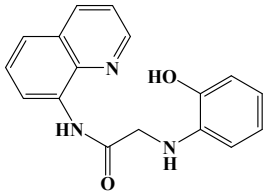	2	0.256	5.18×10^5	20%	[S8]
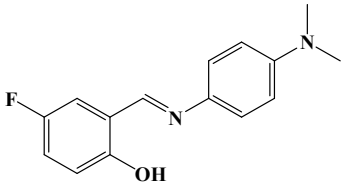	1	0.26	No data	50%	[S9]
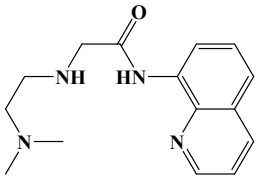	2	0.01	1.3×10^5	bis-tris solution	[S10]

Table S4. Comparison of a few aspects of some recently published Hg-sensors.

Chemosensor	No. of steps for synthesis	Detection Limit (μM)	Binding constant (M^{-1})	Percent of water in solution	Reference
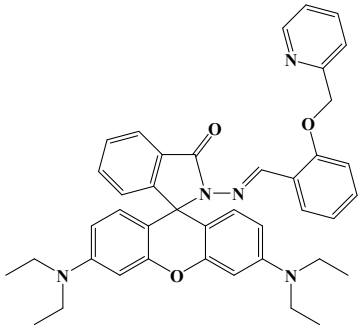	1	3.1	No data	0 (100% ethanol)	[S11]
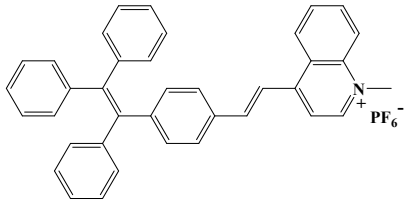	2	0.0718	No data	100%	[S12]
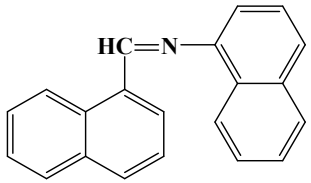	1	0.05595	9.35×10^4	0 (100% DMSO)	[S13]
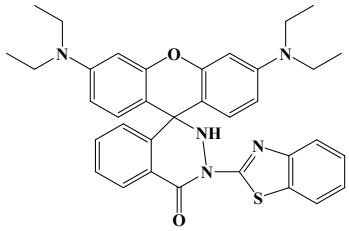	3	No data	1.02×10^6	0 (40% ethanol)	[S14]

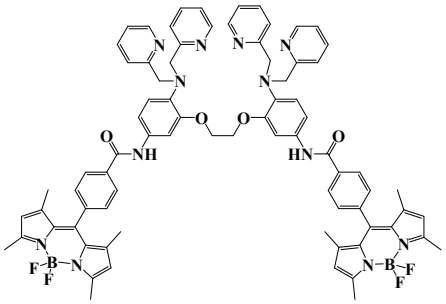	8	0.038	1.8×10^5	0 (20% DMSO)	[S15]
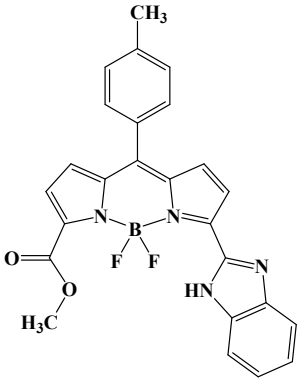	3	0.77	6.18×10^6	0 (70% acetonitrile)	[S16]
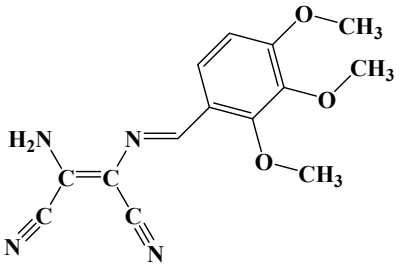	1	1.93	3.62×10^3	20%	[S17]

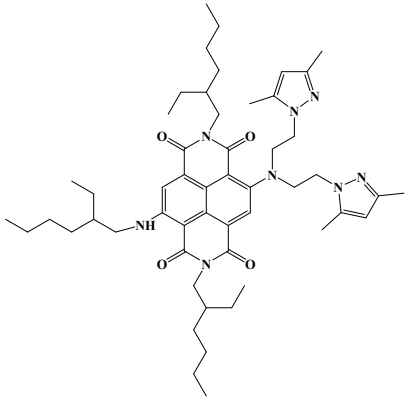	2	1.3	4.24×10^6	0 (acetone)	[S18]
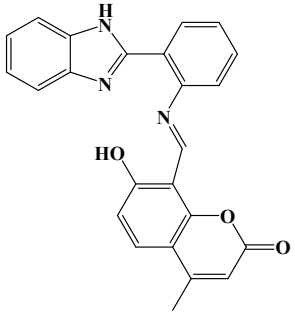	1	0.07	8.75×10^4	0 (100% DMSO)	[S19]
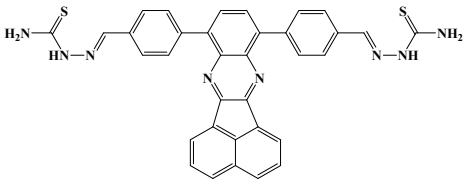	4	0.907	2.51×10^5	10%	[S20]

Table S5. Crystallographic and structural determination data for complexes **MQA-Zn^{2+}** and **MQA-Hg^{2+}**.

	MQA-Zn^{2+}	**MQA-Hg^{2+}**
CCDC No.	1460774	1460775
formula	$C_{17}H_{14}Cl_2N_2OZn$	$C_{17}H_{14}Cl_2N_2OHg$
Mr	398.59	533.79
A cryst syst	Monoclinic	Triclinic
space group	$P2_1/c$	P
a [Å]	7.492(18)	8.108(12)
b [Å]	15.272(4)	8.616(12)
c [Å]	15.500(4)	12.299(18)
α [°]	90	77.039(4)
β [°]	112.715(11)	87.533(4)
γ [°]	90	82.928(4)
Volume [Å^3]	1636.0(7)	830.9(2)
Z	4	2
D_c [g·cm^{-3}]	1.618	2.134
μ [mm^{-1}]	1.832	9.588
F (000)	808	504
Θ range [°]	1.95 – 25.00	1.70 – 25.00
h range	$-8 \le h \le 8$	$-9 \le h \le 9$
k range	$-16 \le k \le 18$	$-10 \le k \le 8$
l range	$-18 \le l \le 18$	$-14 \le l \le 14$
data/restraints/params	2829 / 0 / 208	2920 / 0 / 209
GOF	0.844	0.909
R_1, wR_2[I>2σ(I)][a]	0.0549, 0.1011	0.0452, 0.0766
R_1, wR_2[all data][a]	0.1639, 0.1268	0.0664, 0.0840
$\Delta\rho_{max}$, $\Delta\rho_{min}$ [e·Å^{-3}]	0.523, –0.670	0.930, –1.280

[a] $R_1 = \sum||F_o| - |F_c||/\sum|F_o|$; $wR_2 = [\sum[w\,(F_o^2 - F_c^2)^2]/\sum[\,w\,(F_o^2)^2]]^{1/2}$.

Table S6. Selected bond distances (Å) and angles (°) for **MQA-Zn^{2+}** and **MQA-Hg^{2+}**.

Parameter	**MQA-Zn^{2+}**	**MQA-Hg^{2+}**
M(1)-N(1)	2.135(5)	2.397(7)
M(1)-N(2)	2.073(5)	2.359(7)
M(1)-Cl(1)	2.226(2)	2.384(3)
M(1)-Cl(2)	2.218(2)	2.419(3)
M(1)-O(1)	2.393(4)	2.668(6)
N(2)-C(10)	1.296(8)	1.261(11)
N(2)-M(1)-N(1)	78.6(2)	71.7(2)
N(1)-M(1)-Cl(1)	108.40(15)	111.12(18)
N(2)-M(1)-Cl(1)	110.51(15)	131.60(18)
N(1)-M(1)-Cl(2)	104.57(15)	107.20(18)
N(2)-M(1)-Cl(2)	128.33(16)	101.94(18)
Cl(2)-M(1)-Cl(1)	116.56(8)	121.09(10)
N(1)-M(1)-O(1)	147.08(19)	129.2(2)
N(2)-M(1)-O(1)	70.08(18)	62.8(2)
Cl(1)-M(1)-O(1)	92.32(13)	85.32(16)
Cl(2)-M(1)-O(1)	87.57(12)	103.11(16)
C(12)-O(1)-M(1)	114.1(4)	115.9(5)

C(17)-O(1)-M(1)	125.3(4)	123.4(5)
C(1)-N(1)-M(1)	112.2(4)	112.7(6)
C(5)-N(1)-M(1)	129.8(5)	126.3(6)
C(10)-N(2)-M(1)	115.2(4)	114.3(6)
C(11)-N(2)-M(1)	122.8(4)	122.7(6)

Supporting References

[S1] Zhou, Y.; Li, Z. X.; Zang, S. Q.; Zhu, Y. Y.; Zhang, H. Y.; Hou, H. W.; Mak, T. C. W. A Novel Sensitive Turn-on Fluorescent Zn^{2+} Chemosensor Based on an Easy to Prepare C_3-Symmetric Schiff-Base Derivative in 100% Aqueous Solution. *Org. Lett.* **2012**, *14*, 1214−1217.

[S2] Yang, M. D.; Zhang, Y.; Zhu, W. J.; Wang, H. Z.; Huang, J.; Cheng, L. H.; Zhou, H. P.; Wu, J. Y.; Tian. Y. P. Difunctional Chemosensor for Cu(II) and Zn(II) Based on Schiff Base Modified Anthryl Derivative with Aggregation-Induced Emission Enhancement and Piezochromic Characteristics. *J. Mater. Chem. C* **2015**, *3*, 1994–2002.

[S3] Goswami, S.; Das, A. K.; Aich, K.; Manna, A.; Maity, S.; Khanra, K.; Bhattacharyya. N. Ratiometric and Absolute Water-Soluble Fluorescent Tripodal Zinc Sensor and Its Application in Killing Human Lung Cancer Cells. *Analyst* **2013**, *138*, 4593–4598.

[S4] Song, E. J.; Kang, J.; You, G. R.; Park, G. J.; Kim, Y.; Kim, S. J.; Kim, C.; Harrison, R. G. A Single Molecule that Acts as a Fluorescence Sensor for Zinc and Cadmium and a Colorimetric Sensor for Cobalt. *Dalton Trans.* **2013**, *42*, 15514–15520.

[S5] Sarkar, D.; Pramanik, A. K.; Mondal. T. K. Coumarin Based Dual Switching Fluorescent 'turn-on' Chemosensor for Selective Detection of Zn^{2+} and HSO_4^-: an Experimental and Theoretical Study. *RSC Adv.* **2014**, *4*, 25341–25347.

[S6] Mati, S. S.; Chall, S.; Konar, S.; Rakshit, S.; Bhattacharya, S. C. Pyrimidine-Based Fluorescent Zinc Sensor: Photo-Physical Characteristics, Quantum Chemical Interpretation and Application in Real Samples. *Sens. Actuators B* **2014**, *201*, 204–212.

[S7] Tang, L. J.; Dai, X.; Zhong, K. L.; Wu, D.; Wen. X. A Novel 2,5-diphenyl-1,3,4-oxadiazole Derived Fluorescent Sensor for Highly Selective and Ratiometric Recognition of Zn^{2+} in Water through Switching on ESIPT. *Sens. Actuators B* **2014**, *203*, 557–564.

[S8] Yue, Y. Y.; Dong, Q.; Zhang, Y. J.; Sun, Y. Y.; Gong, Y. J. A Highly Selective "turn-on" Fluorescent Chemosensor Based on 8-Aminoquinoline for Detection of Zn^{2+}. *Anal. Methods* **2015**, *7*, 5661–5666.

[S9] Yan, L. Q.; Qing, T. T.; Li, R. J.; Wang, Z. W.; Qi, Z. J. Synthesis and Optical Properties of Aggregation Induced Emission (AIE) Molecules Based on the ESIPT Mechanism as pH- and Zn^{2+}-Responsive Fluorescent Sensors. *RSC Adv.* **2016**, *6*, 63874–63879.

[S10] Park, G. J.; Lee, J. J.; You, G. R.; Nguyen, L. T.; Noh, I.; Kim, C. A Dual Chemosensor for Zn^{2+} and Co^{2+} in Aqueous Media and Living Cells: Experimental and Theoretical Studies. *Sens. Actuators B* **2016**, *223*, 509–519.

[S11] Li, L. Q.; Yuan, L.; Liu, Z. H. A Highly Selective Turn on Fluorescence Sensor for Hg^{2+} Based on Rhodamine Derivative. *J. Fluoresc.* **2014**, *24*, 1357–1361.

[S12] Zhang, R. X.; Li, P. F.; Zhang, W. J.; Li, N.; Zhao, N. A Highly Sensitive Fluorescent Sensor with Aggregation-Induced Emission Characteristics for the Detection of Iodide and Mercury Ions in Aqueous Solution. *J. Mater. Chem. C* **2016**, *4*, 10479–10485.

[S13] Wei, T. B.; Gao, G. Y.; Qu, W. J.; Shi, B. B.; Lin, Q.; Yao, H.; Zhang, Y. M. Selective Fluorescent Sensor for Mercury(II) Ion Based on an Easy to Prepare Double Naphthalene Schiff Base. *Sens. Actuators B* **2014**, *199*, 142–147.

[S14] Yang, Z.; Hao, L. K.; Yin, B.; She, M. Y.; Obst, M.; Kappler, A.; Li, J. L. Six-Membered Spirocycle Triggered Probe for Visualizing Hg^{2+} in Living Cells and Bacteria–EPS–Mineral Aggregates. *Org. Lett.* **2013**, *15*, 4334−4337.

[S15] Maity, S. B.; Banerjee, S.; Sunwoo, K.; Kim, J. S.; Bharadwaj, P. K. A Fluorescent Chemosensor for Hg^{2+} and Cd^{2+} Ions in Aqueous Medium under Physiological pH and Its Applications in Imaging Living Cells. *Inorg. Chem.* **2015**, *54*, 3929−3936.

[S16] Madhu, S.; Sharma, D. K.; Basu, S. K.; Jadhav, S.; Chowdhury, A.; Ravikanth, M. Sensing Hg(II) in Vitro and in Vivo Using a Benzimidazole Substituted BODIPY. *Inorg. Chem.* **2013**, *52*, 11136−11145.

[S17] Huo, Y. P.; Wang, S. Y.; Lu, T. H.; Pan, C. Q.; Lu, Y. J.; Yang, X. H.; Hu, D. P.; Hu, S. Highly Selective and Sensitive Colorimetric Chemosensors for Hg^{2+} Based on Novel Diaminomaleonitrile Derivatives. *RSC Adv.* **2016**, *6*, 5503–5511.

[S18] Zong, L. Y.; Xie, Y. J.; Li, Q. Q.; Li, Z. A New Red Fluorescent Probe for Hg^{2+} based on Naphthalene Diimideand Iits Application in Living Cells, Reversibility on Strip Papers. *Sens. Actuators B* **2017**, *238*, 735–743.

[S19] Gao, Y. L.; Zhang, C.; Peng, S. W.; Chen, H. Y. A Fluorescent and Colorimetric Probe Enables Simultaneous Differential Detection of Hg^{2+} and Cu^{2+} by Two Different Mechanisms. *Sens. Actuators B* **2017**, *238*, 455–461.

[S20] Feng, L.; Shi, W.; Ma, J. C.; Chen, Y. B.; Kui, F.; Hui, Y. H.; Xie, Z. F. A Novel Thiosemicarbazone Schiff Base Derivative with Aggregation-Induced Emission Enhancement Characteristics and Its Application in Hg^{2+} Detection. *Sens. Actuators B* **2016**, *237*, 563–569.